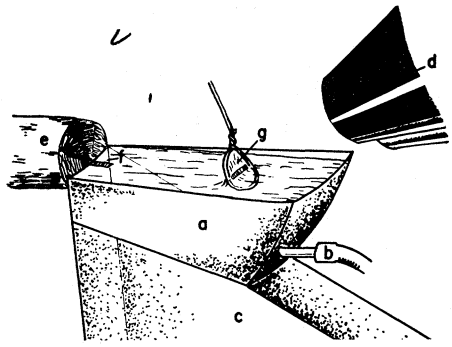

Fig. 2. Equipment used to collect serial sections: *a*, collecting trough; *b*, plastic tube connecting the trough with the hypodermic syringe; *c*, glass knife; *d*, dissecting microscope; *e*, methacrylate block; *f*, ribbon of serial sections; *g*, Formvar-coated loop

holding the sections. The loop is attached to the disk so that the sections are located in the center of the opening. By manipulation of the disk on the microscope stage, the ribbon of sections is optically superimposed over a slit in the grid. The condenser mount is raised to bring the grid and the Formvar film into contact; further elevation causes the rod with the grid to pass through the wire loop. The Formvar film, including the sections located over one of the slits of the grid, is firmly attached in this manner to the surface of the grid. The uninterrupted ribbon of sections is then ready for examinations in the electron microscope.

The electron micrographs in Fig. 1 show such a series of sections cut with a Porter and Blum (*1*) microtome and mounted on a single grid. These 18 sections, representing a total thickness of less than 2 μ, demonstrate the potentialities of using serial sections for determining the three-dimensional distribution of cytoplasmic structures such as the endoplasmic reticulum and secretion granules. For example, a single cross section of the endoplasmic reticulum shows lines that might be thought to represent either isolated fibrils or walls of tubules. In serial sections, however, the double lines may be followed from section to section indicating that they represent membranes making up a complex structure of interconnected curved lamellae. Gaps in these lines suggest holes in the membranes. The serial sections of Fig. 1 also reveal that the secretion granules are essentially spherical: the progressive changes in diameter in succeeding sections, such as can be seen in the two granules at the bottom of sections 1 to 13, indicate a succession of cuts through a radially symmetrical object. These examples illustrate the usefulness of serial sections in working out the three-dimensional relationships of newly observed cellular constituents whose structure is not obvious in individual sections.

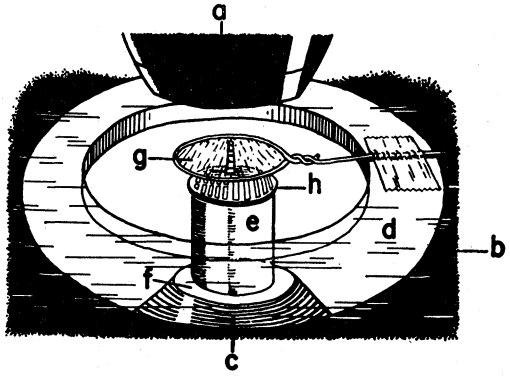

Fig. 3. Equipment used to transfer the serial sections to a Sjöstrand grid: *a*, microscope objective lens; *b*, microscope stage; *c*, condenser; *d*, large plastic disk; *e*, ⅛-in. plastic rod; *f*, plastic disk to support rod; *g*, loop with serial sections; *h*, Sjöstrand grid.

Another advantage of serial sectioning for electron microscopy is that it will aid in locating specific constituents within cells, which in the past has been a matter of chance. The method described here will permit collection of serial sections through an entire cell. Only a few of these need be examined to select the particular sections containing the organelle of special interest for intensive three-dimensional study.

References and Notes

* Lalor Foundation fellow, University of Pennsylvania. Grateful acknowledgment is made to the Lalor Foundation. Present address: Department of Genetics, Carnegie Institution, Cold Spring Harbor, L.I., N.Y.

1. K. R. Porter and J. Blum, *Anat. Record* **117**, 685 (1953).
2. F. S. Sjöstrand, *Experientia* **9**, 114 (1953).

3. These studies were aided by a contract (NR 135-197) between the Office of Naval Research, Department of the Navy, and the University of Pennsylvania.

4. G. E. Palade, *J. Exptl. Med.* **95**, 285 (1952).

14 September 1954.

Theoretical Rate Equation for World-Record Running Speeds

Franklin M. Henry

Department of Physical Education, University of California, Berkeley

Lietzke (*1*) has reviewed the various attempts that have been made since 1905 to formulate a mathematical description of the time-speed-distance relationships in world-record performances. In the most recent of these, Francis in 1943 used a semilogarithmic hyperbola (*2*) for the distance range ¼ to 10 mi. Lietzke did not think the fit was satisfactory and returned to the simple 1905 parabola with a revision of the curve constants. He has been remarkably successful in applying this curve (distance = at^k) to the known records for walking, running from 880 yd to the 26-mi marathon, swimming, and both horse and automobile racing. Nevertheless, his equation does not hold for the shorter distances in either swimming or running, and the rate equation he derives from it, for human running, does not fit the observed values closely for any distance range. His rate curve is therefore a smooth curve between the observed points and is not a graph of the equation.

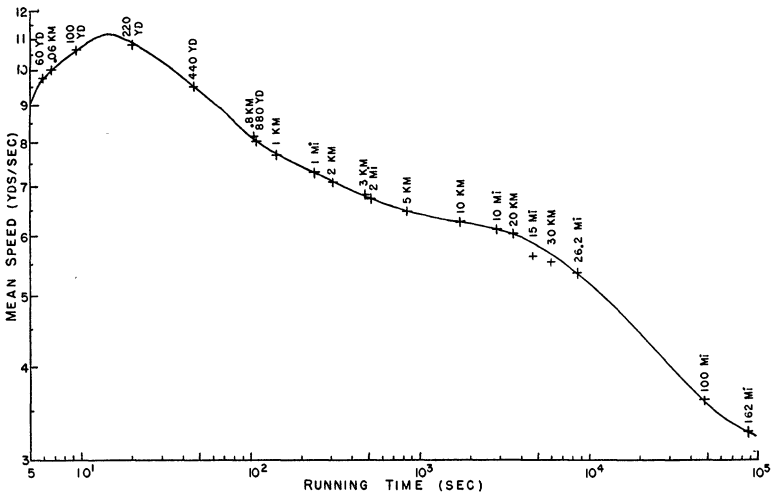

Fig. 1. Rate vs. time curve for 1954 world records in running.

Table 1. Curve constants.

Item	a (yd/sec)	k (sec)	Half-time
Energy loss	−13.10	2.48×10^{-1}	2.79 sec
Alactate	4.80	2.53×10^{-2}	27.4 sec
Lactate	1.70	3.45×10^{-3}	3.35 min
Glycogen	2.96	5.88×10^{-5}	3.27 hr
Fat, etc.	3.64	1.234×10^{-6}	6.5 days

It can be postulated that the maximum speed in running is limited by the energy reserves available for conversion into work, and that each of these resources begins to be depleted from the very beginning of the race in accord with an exponential law. These resources consist of the alactate and lactate oxygen debts, the glycogen reserve, body fat, and eventually body protein.

Also to be considered is the energy-loss factor, proportional to speed, that was at one time thought to be due to muscle viscosity. It is now known that the loss must be explained in more complicated terms. However, it is possible to represent this factor as a simple exponential term carrying a negative sign (*3*).

The available data do not permit an estimate of the role of protein depletion as an energy source in running, but it is doubtful that it is quantitatively important under ordinary circumstances. The rate of depletion of the other energy sources can be guessed at from various types of information—the half-times would be expected to be several days for fat, several hours for glycogen, 3 to 5 min for the lactate debt, and about 30 sec for the alactic debt.

Figure 1 shows a log-by-log plot of the equation

$$dy/dt = a_1e^{-k_1t} + a_2e^{-k_2t} + a_3e^{-k_3t} + a_4e^{-k_4t} + a_5e^{-k_5t},$$

using the curve constants given in Table 1. It will be observed that each of the rate coefficients k is of a different order of magnitude. It may also be noted that a parabolic rate equation would plot in a straight line in this figure. Details of the method of curve-fitting and explanation of the time constants are being published elsewhere (*4*).

References

1. M. H. Lietzke, *Science* **119**, 333 (1954).
2. A. W. Francis, *ibid.* **98**, 315 (1943).
3. F. M. Henry, *Research Quart.* **22**, 409 (1951).
4. ———, *ibid.* **26**, in press.

7 September 1954.

Comments and Communications

Avelinoite, a New Hydrous Sodium Ferric Phosphate Mineral from Minas Gerais, Brazil

Avelinoite, a hydrous sodium ferric phosphate, is the sixth new phosphate mineral described since 1949 from the granite pegmatite at the Sapucaia pegmatite mine, Minas Gerais, Brazil. [See *Science* **119**, 739 (1954) and Am. Mineralogist **34**, 541 (1949); **38**, 263, 1126 (1953)]. The mineral is named in honor of Avelino Ignacio de Oliveira, eminent Brazilian geologist and director of the National Department of Mineral Production, Rio de Janeiro.

Avelinoite occurs as yellow well-formed crystals, less than 1 mm in length, on cavity walls in altered phosphate, principally frondelite. Its specific gravity is 3.08 and its optical properties are: uniaxial, negative; $\omega = 1.803$; $\varepsilon = 1.769$. The crystals are assigned to the tetragonal pyramidal class. The basal pinacoid {001} and 1st-order pyramid {113} are prominent forms; the 2nd-order pyramid {012} is poorly developed. The axial ratio is $a : c = 1 : 2.650$; ρ (calc.) for {012} is 52°58′ and ρ for {113} is 51°20′.

Single crystal x-ray studies define the space group to be $P4_1$ (C_4^2). The cell size is $a_0 = 7.32$, $c_0 = 19.4$ A. On the powder pattern strong reflections occur with d-spacings of 4.85, 3.60, 3.186, 3.101, 2.913, 2.658, 2.209, 2.181, and 2.020 A. The unit cell contains $Na_4Fe_{12}^{III}(PO_4)_8(OH)_{16} \cdot 8H_2O$.

The chemical analysis shows: Na_2O, 4.70; K_2O, 0.63; MnO, 0.99; CaO, 0.10; FeO, none; Fe_2O_3, 47.87; Al_2O_3, 1.36; P_2O_5, 29.06; H_2O, 14.45; insol.,